DOI:10.22337/2587-9618-2026-22-1-104-117

NONLINEAR DYNAMIC ANALYSIS OF THE STEEL-RUBBER VIBRATION ISOLATORS WITH PERFORATION

Vladimir L. Mondrus [1], Dmitry K. Sizov [2], Timofei M. Kvasnikov [1]
[1] National Research Moscow State University of Civil Engineering, Moscow, RUSSIA
[2] OOO "Vibroseismozastchita", Moscow, RUSSIA

Abstract: The paper presents a comparative study of nonlinear dynamic analyses of perforated and non-perforated steel–rubber vibration isolators. Particular emphasis is placed on the nonlinear response of rubber, incorporating hyperelasticity (via the Mooney–Rivlin model) and viscoelasticity (through a Prony series), under static preloading conditions. The computational methodology is implemented in Python, integrating the finite element method (FEM), the Newmark-β time integration scheme for dynamic equilibrium, and a Newton–Raphson iterative solver enhanced with line search.

Keywords: vibration isolation, steel-rubber vibration isolator with holes, Mooney–Rivlin model, Prony series, Newmark-β method

НЕЛИНЕЙНЫЙ ДИНАМИЧЕСКИЙ АНАЛИЗ ПЕРФОРИРОВАННЫХ РЕЗИНОМЕТАЛЛИЧЕСКИХ ВИБРОИЗОЛЯТОРОВ

В.Л. Мондрус [1], Д.К. Сизов [2], Т.М. Квасников [1]
[1] Национальный исследовательский Московский государственный строительный университет (НИУ МГСУ), г. Москва, РОССИЯ
[2] ООО «Вибросейсмозащита», г. Москва, РОССИЯ

Аннотация: В статье представлены результаты сравнения нелинейного динамического анализа резинометаллических виброизоляторов с перфорациями и без. Особое внимание уделяется нелинейному поведению резины с учётом гиперупругости (модель Муни-Ривлина), вязкоупругости (ряды Прони) при статическом предварительном нагружении. Расчётная методика реализована с помощью языка программирования Python с применением метода конечных элементов, схемы Ньюмарка и итерационного алгоритма Ньютона-Рафсона с line search

Ключевые слова: виброизоляция, резинометаллический виброизолятор с отверстиями, модель Муни-Ривлина, ряды Прони, метод Ньюмарка-β

1. INTRODUCTION

Vibrations generated by underground rail transport pose a serious threat to the serviceability of buildings located in close proximity to subway tunnels. These vibrations propagate through the soil and are transmitted to building structures via their foundations. The spectral composition of the excitation is determined by several mechanisms: the relative motion of the train car body and its suspension system, wheel bounce on the rails, and the resistance to motion caused by the wheel-rail contact surface.

Introducing perforations into the structure of a vibration isolator allows for the tuning of its dynamic characteristics and broadening of its isolation band. However, this significantly complicates the calculation of its stress-strain state. Furthermore, rubber exhibits pronounced hyperelastic and viscoelastic behavior, which necessitates the use of advanced numerical analysis methods that account for large deformations, nonlinear

material models, and the interaction between prestress and dynamic loading.

The objective of this work is the nonlinear dynamic analysis of three types of rubber-metal vibration isolators. The methodology is based on a multi-step calculation procedure: a static analysis with a preload representing the load from a portion of the building, followed by a dynamic analysis employing the Newton-Raphson algorithm with line search and implicit Newmark time integration.

The computational core of the code, written in the Python programming language, utilizes the NumPy and SciPy libraries. The NumPy library provides efficient storage for dense arrays and enables vectorized operations, while the scipy.sparse module is used to store the global stiffness and mass matrices, which are highly sparse in finite element analysis (FEA) problems. To solve the systems of linear algebraic equations at each Newton-Raphson iteration, efficient direct solvers available in scipy.sparse.linalg are employed.

The general implementation algorithm in Python is as follows:

Mesh generation was performed directly in Python, with the capability to export in VTK format for subsequent validation in ParaView. The domain was discretized using cubic HEX8 elements. Based on this data, a material class is created, defining functions to compute the internal force vector and tangent stiffness matrices, incorporating the hyperelastic Mooney-Rivlin model and viscoelasticity implemented via Prony series. The next step is the global assembly procedure, which sums the contributions of individual finite elements into the overall sparse system matrix.

A key stage prior to the dynamic analysis is the preliminary static calculation, where the load is applied in increments, and the nonlinear system of equations at each step is solved using the Newton-Raphson method. This allows for the determination of the initial deformed state and the updating of the tangent stiffness matrix to account for the resulting geometric nonlinearity.

The computational process concludes with the application of the Newmark-β method for dynamic analysis. At each time step t_{n+1}, a nonlinear system of dynamic equilibrium equations is formulated and solved using the iterative Newton-Raphson method. Within each iteration, the current kinematic parameters are estimated using the Newmark relationships, after which the geometry, stresses, and tangent stiffness matrix are updated. Upon achieving convergence, the material history is updated, and the results are saved for post-processing [1-4].

2. RESEARCH METHODS

Initial Excitation and Isolator Geometry

The challenge of correctly selecting the resonant frequency of a vibration isolator requires a deep understanding of the spectral composition of the excitation generated by a shallow subway system. The analysis was performed by processing data obtained from a three-channel vibration meter (sensors Kn1, Kn2, Kn3) in octave frequency bands from 2 to 250 Hz, located near the "Akademicheskaya" subway station. Processing of the experimental data showed (Figure 2) that the spectrum of the vibration signal has a distinctly uneven character with several key peaks. The highest energy saturation of the signal was recorded in the low-frequency range, which is characteristic of the impact of rolling stock on the soil mass. The dominant peak is in the octave band with a center frequency of 31.5 Hz, where vibration levels reach maximum values (~72 dB). This frequency can be critical for a number of vibration isolation tasks (especially for the natural frequencies of floors and walls), creating a high risk of structural resonance.

In addition to the main peak, significant vibration levels were recorded in the 16 Hz and 63 Hz bands. Specifically, the component at 16 Hz, with a level of about 65 dB, presents a particular challenge for isolation, as it requires the use of vibration isolators with extremely low stiffness.

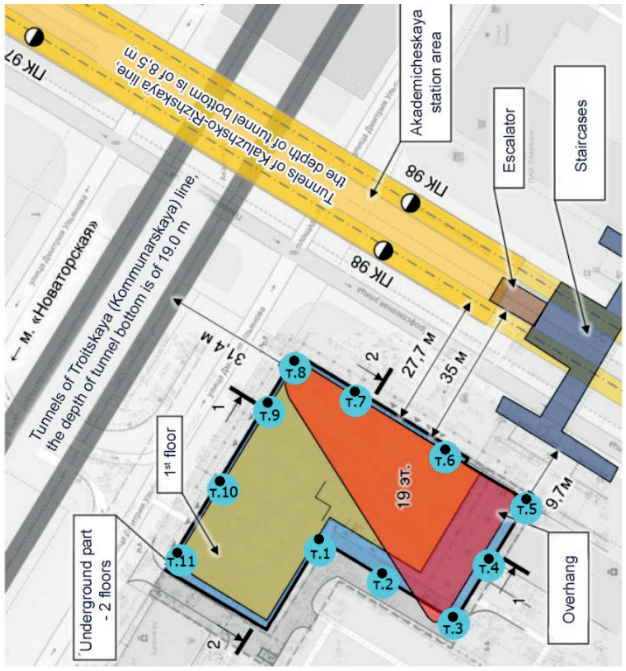


Figure 1. Gauges placement

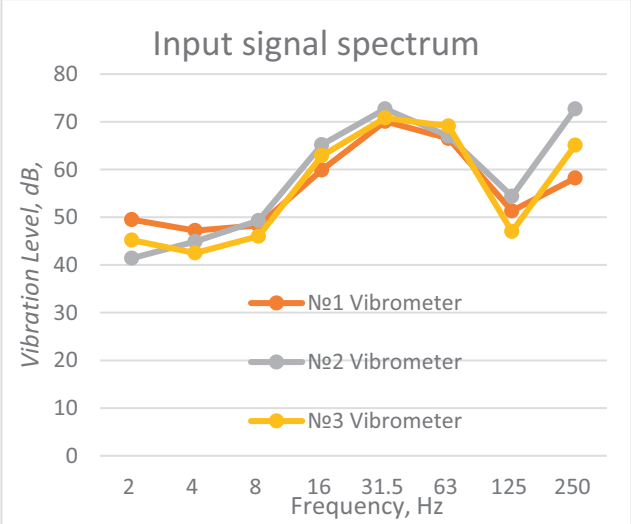


Figure 2. Diagram of the input frequencies spectrum according to gauge indications

Determining the first natural frequency of the system is essential for preventing resonant phenomena. If the first natural frequency of the system is close to the external excitation frequencies, this will lead to a sharp increase in vibration amplitude, intensification of the vibratory impact on structural elements, and potential material failure. [5]

Three variants of the vibration isolator were modeled: a classic rubber-metal type without holes (Type A, Fig. 3, 6), a version with a central through-hole (Type B, Fig. 4, 7), and a modification featuring a central hole plus four additional holes arranged diagonally (Type C, Fig. 5, 8).

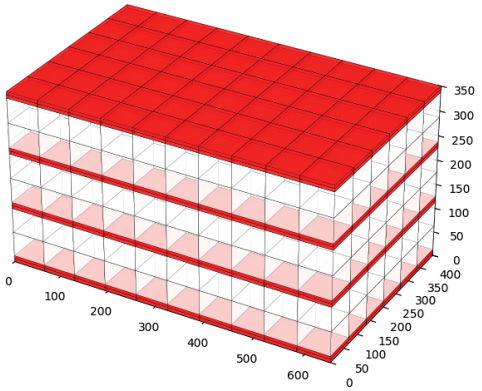


Figure 3. Finite element model of a rubber-metal vibration isolator 650x400x350mm without opening

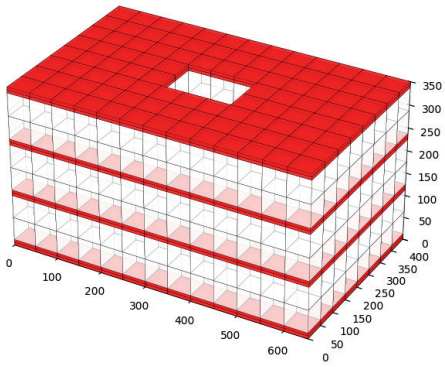


Figure 4. Finite element model of a rubber-metal vibration isolator 650x400x350mm with central opening

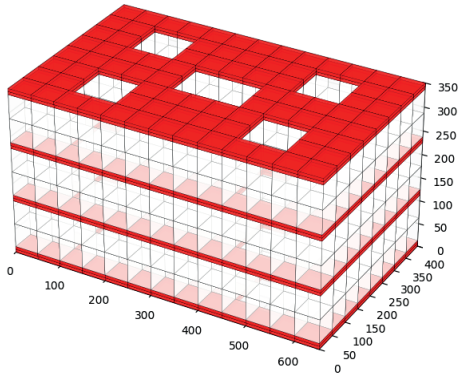


Figure 5. Finite element model of a rubber-metal vibration isolator 650x400x350mm with five openings

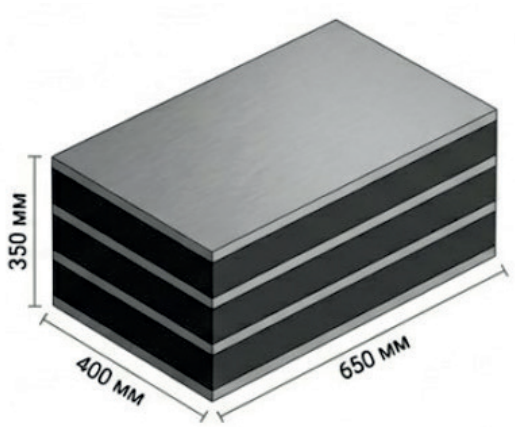


Figure 6. 3D view of a rubber-metal vibration isolator 650x400x350mm without opening

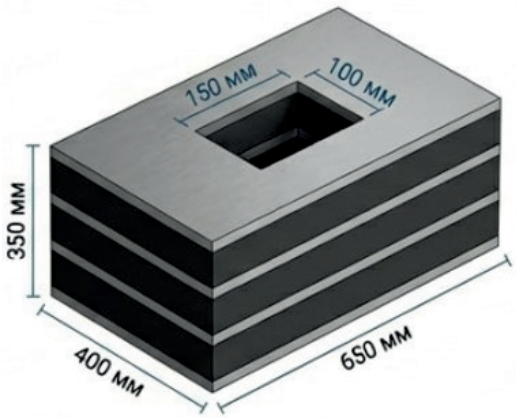


Figure 7. 3D view of a rubber-metal vibration isolator 650x400x350mm with central opening

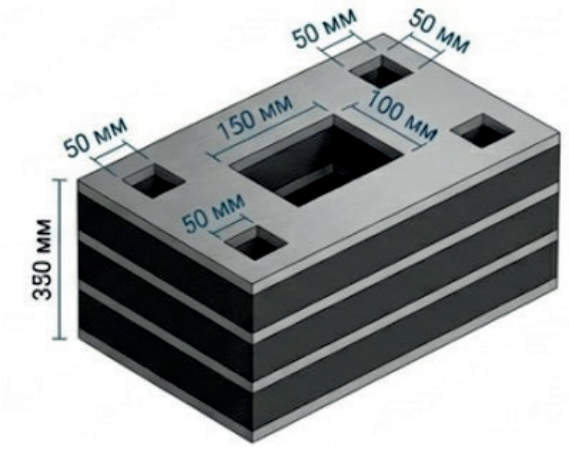


Figure 8. 3D view of a rubber-metal vibration isolator 650x400x350mm with five openings

The overall dimensions of the vibration isolator are 650 × 400 × 350 mm. The structure consists of alternating layers: steel plates with a thickness of 12.5 mm and rubber layers with a thickness of 100 mm.

The dimensions of the central hole are set at 150 × 100 mm, while the dimensions of the staggered holes are set at 50 × 50 mm.

The steel plates are defined by the following parameters: $E = 2 \cdot 10^{11}$ Pa, $\nu = 0.3$, and a density of $\rho = 7000$ kg/m³.

Hyper elastic behavior

The hyper elastic behavior of the rubber is described using the strain energy density function in the Mooney-Rivlin model:

$$W = C_{10}(I_1 - 3) + C_{01}(I_2 - 3) + \frac{1}{D_1}(J_{el} - 1)^2 \quad (1)$$

where:

$I_1 = tr(C)$ is the first invariant of the right Cauchy-Green deformation tensor

$I_2 = \frac{1}{2}[(tr(C))^2 - tr(C^2)]$ is the second invariant

$J_{el} = \sqrt{\det(C)}$ is the volumetric tension

$C_{10} = 0.35$ MPa and $C_{01} = 0.12$ MPa are the material constants.

The first sum describes the deviatoric part of the energy, while the second considers the volumetric part associated with compressibility.

Two-parameter Mooney-Rivlin model (N=1, C_{11}=0) is as follows:

$$W = C_{10}(I_1 - 3) + C_{01}(I_2 - 3) \quad (2)$$

This model is preferable to the simplest neo-Hookean model, since the presence of the term with C_{01} allows one to describe the effect of rubber softening under moderate deformations [6].

Viscoelasticity

The hyper elastic model describes the static behavior of the rubber. However, one of the key functions of a vibration isolator is damping, which in polymers has a viscoelastic nature. This leads to the stress depending not only on the strain, but also on the strain rate and the loading

history. The hyper elastic part describes the equilibrium response; viscoelastic effects are accounted for as deviations from it and contribute to both the static and dynamic response. [7]
In the frequency domain, this is expressed through the complex shear modulus as follows

$$G^*(w) = G'(w) + iG''(w) \quad (3)$$

where G' is the storage modulus (elastic component), and G'' is the loss modulus (viscous component). The tangent of the mechanical loss angle (loss coefficient)

$$tan\delta = G''/G' \quad (4)$$

For the numerical analysis in the time domain, which is necessary for solving nonlinear dynamic problems using Newmark's method, the frequency dependence is transformed into a shear relaxation function $G(t)$. The most convenient approximation is the expansion into Prony series (generalized Maxwell model).
The hyper elastic Mooney-Rivlin model describes the static behavior of rubber; however, a critically important characteristic of a vibration isolator is its damping capacity, which in rubbers has a distinctly viscoelastic nature. These processes cause the stress-strain state to depend not only on the current strain, but also on the entire loading history.
For numerical modeling in the time domain, the frequency dependence of the complex shear modulus $G^*(w)$ is approximated by the shear relaxation function $G(t)$. In the present work, the generalized Maxwell model is used, which is mathematically expressed through Prony series. [8, 9]
The shear relaxation function $G(t)$ is defined by the expression:

$$G(t) = G_0\left[1 - \sum_{k=1}^{N} g_k(1 - e^{-t/\tau_k})\right] \quad (5)$$

where:

- G_0 is the instantaneous shear modulus at t=0, related to the hyper elastic constants by the relation:

$$G_0 = 2(C_{10} + C_{01}) \quad (6)$$

- g_k is the dimensionless relaxation weighting coefficient ($g_k = G_k / G_0$), characterizing the contribution of the k^{th} branch to the overall reduction in rigidity;
- τ_k is the creep times;
- N is the order of the series, i.e., the number of Maxwell branches [10].

The long-term shear modulus (G_∞), which determines the rigidity of rubber after the relaxation processes are completed, is related to the instantaneous modulus by the ratio:

$$G_\infty = G_0[1 - \sum_{k=1}^{N} g_k)] \quad (7)$$

The coefficients are adopted on the basis of identification for high-damping rubbers: $g_1 = 0.436$, $g_2 = 0.058$, $g_3 = 0.005$, $\tau_1 = 9.85$ c, $\tau_2 = 98.5$ c, $\tau_3 = 985.2$ c. [11]

Combined Hyper elastic - Viscoelastic Model for Calculating Stress and the Tangent Stiffness Matrix

In the present study, the hyper elastic and viscoelastic models are used within a unified visco-hyperelastic formulation. The hyper elastic part (Mooney–Rivlin model) defines the equilibrium contribution to the strain energy and determines the static (long-term) stress-strain state, while the viscoelastic part in the form of Prony series describes the deviations from this equilibrium response over time. In practice, this is implemented as follows: at each solution step, based on the known strain tensor, the equilibrium stresses and the material tangent matrix are first computed using the Mooney–Rivlin model (considering G_∞). Subsequently, the non-equilibrium contributions from each branch of the Prony series are added to them. These contributions are determined by their own relaxation equations (internal variables dependent on the strain history). As a result, the total stress tensor represents the sum of the hyper elastic and all viscoelastic components, and the tangent stiffness matrix ($K_{tangent}$) is formed as a superposition of the material stiffness from the Mooney–Rivlin model and additional derivatives

from all branches of the Prony series. This approach ensures the correct accounting of both the instantaneous nonlinear stiffness of the material and the time-dependent relaxation and damping under dynamic loading [12].

Software Architecture and System State Transfer

To implement the numerical modeling in Python, an architecture employing a single class was applied, ensuring the preservation of the system state throughout the entire calculation. Avoiding two independent calculations (static and dynamic) circumvents the difficulties associated with the correct transfer of internal variables describing the history of viscoelastic deformation. Instead, the model implements two sequential solution methods: static and dynamic, both operating on unified variables and classes.

Upon completion of the static loading stage F_{static}, the system records the displacement field, the updated configuration of the mesh nodes, as well as the stress and strain tensors at each integration point. It is important not only to save the tangent stiffness matrix $K_{tangent}$ but also the complete tensor field of stresses. These stresses are responsible for the "geometric stiffness" effect, which modifies the system's response. Omitting information about the initial stresses while preserving only the matrix K would lead to an incorrect calculation of internal forces in subsequent steps of the dynamic analysis.

The transition from statics to dynamics is implemented in Python as a change of solver without recreating the vibration isolator model. The converged solution obtained in the Newton-Raphson loop is accepted as the initial condition t=0 for Newmark's method. This ensures the continuity of the viscoelastic memory: the creep parameters (Prony series terms) accumulated during the static phase are passed as the initial state for the first step of the dynamic calculation.

Accounting for Geometric Nonlinearity

To correctly account for geometric nonlinearity, the stiffness matrix (K) must be recalculated at each time step based on the current nodal coordinates ($x = X + u$). This implies constructing the strain-displacement matrix (B) based on the deformed geometry rather than the original configuration.

The algorithm for a dynamic step includes the following operations:

1. Calculation of total displacements (the sum of static and current dynamic displacements) and updating the coordinates.
2. Updating the matrix (B) and computing the current stresses.
3. Forming the geometric component of the stiffness matrix (K_{geo}), which depends on the current stress-strain state.

The total tangent stiffness matrix is defined as the superposition of the material and geometric components:

$$K_{tangent} = K_{material} + K_{geo} \quad (8)$$

The presence of the component (K_{geo}), reflecting the influence of compressive stresses in the rubber, is critically important for correctly modeling the change in the frequencies of the rubber-metal vibration isolator under load [13].

Structure of the Software Implementation

The practical implementation of the model is built according to a modular scheme:

- **StaticSolver:** Performs the solution of the nonlinear static problem, returning the deformed mesh, the matrix ($K_{tangent}$), the stress field, and the state of the viscoelastic process.
- **State:** A module that receives all current data after each iteration (mesh, matrix K, material properties, internal variables).
- **DynamicSolver:** Conducts the dynamic analysis based on the data from the State module, adds inertial masses to the corresponding degrees of freedom, and implements the numerical time integration procedure using Newmark's method.

The primary requirement is the strict transfer of the mesh and stiffness to the dynamic module.

Applying the load to the top surface exclusively through mass is a necessary condition for generating correct inertial forces, without which a nonlinear dynamic analysis of the vibration isolation is impossible..

3. STATIC ANALYSIS

The static load F_{static} = 2000 kN, simulating the weight of a portion of the building, is applied to the top plate of the vibration isolator as a uniformly distributed load. Given the pronounced geometric nonlinearity (large deformations) and the physical nonlinearity of the hyper elastic material, applying the full load in a single step is impossible due to convergence problems.
To address this issue, an incremental loading procedure was implemented: F_{static} = 2000 kN was divided into 1000 equal substeps (ΔF = 2 kN). At each substep, the equilibrium of the system was sought using the iterative Newton-Raphson method, with a convergence criterion based on the relative norm of the force residual set to 10^{-5}.

Analysis of the Stress-Strain State
As a result of the static calculation, the field of prestresses and the updated (deformed) mesh geometry were obtained. It is this stressed state that determines the tangent stiffness matrix ($K_{tangent}$), which is recorded and passed as the initial condition for the subsequent dynamic analysis [14].

Numerical Implementation of the Nonlinear System Solution using the Newton-Raphson Algorithm
The solution of the system of nonlinear equilibrium equations was carried out using the Newton-Raphson method, incorporating a line search procedure to enhance the stability of the iterative process. The load application procedure was discretized: at each stage, an increment of ΔF = 2 kN was applied, totaling 1000 substeps until the full load value was reached. [15]
During the iterative process, the Jacobian matrix (tangent stiffness matrix) was updated at each step:

$$J = \frac{\partial R}{\partial u} \tag{9}$$

The force residual vector (R) was defined as the difference between the external loads and the internal reaction forces of the system:

$$R = F_{ext} - F_{int}(u) \tag{10}$$

The computational algorithm within each loading substep was implemented according to the following scheme:

1. Residual Calculation. The current force imbalance vector is determined as follows:

$$R_i = F_{ext} - F_{int}(u_i) \tag{11}$$

2. Convergence Check. The norm of the residual is evaluated against the relative convergence tolerance ε_{rel}:

$$\frac{\|R_i\|}{\|F_{ext}\|} < \varepsilon_{rel} \tag{12}$$

where the convergence tolerance is taken as $\varepsilon_{rel} = 10^{-5}$

3. Solving the Linearized System. The displacement increment vector is computed as follows:

$$J_i \Delta u_i = R_i \tag{13}$$

4. Line Search (State Update). The current nodal coordinates are corrected using a step size α:

$$u_{i+1} = u_i + \alpha \Delta u_i \tag{14}$$

The backtracking method was used to determine the parameter α. In cases where the full algorithm step (α = 1) did not lead to a decrease in the residual, a step reduction algorithm with a factor of 0.5 was activated.

Algorithm Efficiency
Analysis of the numerical simulation results demonstrated the high efficiency of the specified algorithm:

- The number of Newton-Raphson iterations per loading substep decreased from 18–22 to 7–12.
- Cases of solution divergence in situations requiring step damping ($\alpha < 0.3$) were eliminated.

Transfer to Dynamic Analysis

The modeling of the inertial properties of the system is carried out by modifying the global matrices and vectors before initializing the dynamic loop. During the static calculation stage, the external force vector (F_{ext}) is formed, simulating the gravitational load on the top nodes, and the system of equilibrium equations is solved, with inertial terms excluded from these equations [16].

Before starting the dynamic step, a procedure for redefining the system of equations is performed:

1. The components of the external force vector (F_{ext}) corresponding to the static pressure are zeroed out, as this load transitions into the category of inertial forces.
2. The global mass matrix (M) is modified. The calculated equivalent mass is distributed among the corresponding nodes of the top face of the isolator.

In the Python code, this is implemented by adding lumped masses to the diagonal entries of the global matrix.

The equation of motion is written as a balance of inertial and internal forces:

$$M\ddot{u} + F_{int}(u, \dot{u}, history) = 0 \qquad (15)$$

The internal force vector (F_{int}) includes stresses from both the hyper elastic Mooney-Rivlin model and the viscoelastic model. An explicit damping matrix C is not used, as energy dissipation arises automatically in the calculation of F_{int} due to the dependence of stresses on the strain history. The damping of viscoelastic materials is strongly frequency-dependent. The Rayleigh matrix ($C = \alpha M + \beta K$) assumes damping proportional to mass or stiffness, which provides a very rough, non-physical approximation of the frequency dependence [17, 18].

4. DYNAMIC ANALYSIS

Numerical integration of the equations of motion was performed using the implicit Newmark scheme. The parameters $\beta = 0.25$ and $\gamma = 0.5$ were used, corresponding to the constant average acceleration scheme, which ensures stability and the absence of numerical dissipation.

The time integration step was set to $\Delta t = 10^{-4}$ s. The choice of step size is justified by the accuracy criterion for reproducing wave processes:

$$f_{max}\Delta t < 0.1 \qquad (16)$$

where f_{max} = 31.5 Hz is the upper bound of the frequency range of the external excitation.

The kinematic parameters of the system at the new time step (n+1) are determined through the recurrence relations:

Displacement prediction

$$u_{n+1} = u_n + \Delta t\dot{u}_n + \left(\frac{1}{2} - \beta\right)\Delta t^2\ddot{u}_n + \beta\Delta t^2\ddot{u}_{n+1} \qquad (17)$$

Velocity prediction

$$\dot{u}_{n+1} = \dot{u}_n + (1-\gamma)\Delta t\ddot{u}_n + \gamma\Delta t\ddot{u}_{n+1} \qquad (18)$$

To solve the nonlinear system of dynamic equilibrium equations at each time step, the iterative Newton–Raphson method was employed.

Linearization of the equation

$$M\ddot{u} + F_{int}(u, \dot{u}, history) = 0 \qquad (19)$$

within the framework of the Newmark scheme leads to the formation of an effective stiffness matrix:

$$K_{eff} + K_{tangent} + \frac{1}{\beta\Delta t^2}M \qquad (20)$$

where the tangent matrix is as follows:

$$K_{tangent} = \frac{\partial F_{int}}{\partial u} \qquad (21)$$

It includes:

- the material component from the equilibrium stress (Mooney–Rivlin),
- the material contributions from all branches of the Prony series,
- the geometric stiffness resulting from pre-existing stresses.

The damping matrix (C) is not formed explicitly, as the energy dissipation properties of the system are fully accounted for within the nonlinear vector (F_{int}) [19].

The line search procedure is activated if the norm of the residual at the new iteration increases compared to the previous one or decreases insufficiently rapidly (by less than a specified tolerance).

$$\|R_{i+1}\| > \|R_i\| \tag{22}$$

5. RESULTS AND DISCUSSION

Vibration Isolator Settlement

At the moment of load application from the weight of the building portion (t=0), the vertical settlement (u_z) values of the top face of the vibration isolator were obtained. The introduction of perforation expectedly reduced the vertical stiffness of the element, leading to an increase in static deformation:

- Type A (No perforation): Settlement amounted to -10.2 mm. The vibration isolator demonstrates maximum stiffness.
- Type B (1 central hole): Settlement increased to -14.5 mm. The reduction in cross-sectional area led to a moderate increase in settlement.
- Type C (5 holes: 1 center + 4 staggered): Settlement amounted to -22.1 mm. Significant perforations substantially reduced the stiffness of the vibration isolator, providing the softest response to the static load.

Displacement Time History

At time t=0, the settlements start from the static settlement values (-10.2, -14.5, and -22.1 mm, respectively), rather than from zero, which confirms the correct transfer of the stress-strain state from the Static module to the Dynamic module.

Spectral Analysis and Determination of Natural Frequencies

To identify the dynamic characteristics of the vibration isolators in their working (compressed) state, the time histories of vertical displacements ($u_z(t)$), obtained from numerical simulation of the system's free damped vibrations after being displaced from the static equilibrium position, were processed.

Dynamic Analysis

The dynamic analysis of the loaded system revealed a dependence between the perforation types and the dynamic characteristics of the vibration isolator:

- **Type A (Solid):** The spectral peak was recorded at a frequency of **9.50 Hz**.
- **Type B (1 hole):** The introduction of a central channel led to a slight decrease in stiffness, with a frequency of **9.43 Hz**. This minimal difference (less than 1%) is explained by the fact that removing material from the center reduced the vertical stiffness of the system, but simultaneously decreased the associated oscillating mass of the rubber, resulting in the stiffness-to-mass ratio remaining practically unchanged.
- **Type C (5 holes):** The maximum reduction in dynamic stiffness was recorded for the configuration with five holes. The frequency shifted to **8.06 Hz** (a reduction of ~15% relative to Type A).

The significant frequency drops for Type C by 1.44 Hz relative to the solid specimen. This confirms the effectiveness of perforation for reducing support stiffness without loss of stability.

Vibration Isolation Efficiency

The evaluation of vibration protection properties was carried out for the dominant frequency of the external excitation f_{ext} = 31.5 Hz, corresponding to the maximum spectral density of the signal generated by the subway.

According to the theory of linear vibration isolation, the transmission ratio (TR) is determined by the ratio of the excitation frequency to the natural frequency of the system [20]:

$$\eta = f_{ext}/f_n \quad (23)$$

Effective isolator operation is ensured under the condition:

$$\eta > \sqrt{2} \quad (24)$$

Comparative Efficiency Calculation:
For Type A (Solid):
Frequency ratio η = 31.5 / 9.50 ≈ 3.32.
The system is in the vibration isolation zone. The theoretical transmission ratio is TR ≈ 0.10.
For Type B (1 hole):
Frequency ratio η = 31.5 / 9.43 ≈ 3.34.
The indicators are practically identical to the solid vibration isolator. A hole only in the central zone had a minimal impact on the global vertical mode, providing only a symbolic gain in isolation efficiency (less than 1%).
For Type C (5 holes):
Due to the significant reduction in natural frequency, the ratio η increased to 31.5 / 8.06 ≈ 3.91. The increase in frequency detuning leads to a decrease in the theoretical transmission ratio to TR ≈ 0.07. This provides an additional reduction in vibration levels compared to the base variant.

Analysis of Time Histories
Numerical simulation in the time domain confirmed the modal analysis data. For all isolator types, a significant suppression of acceleration amplitudes is observed. However, Type C demonstrates qualitatively different response dynamics: due to its "softer" structure and frequency of 8.06 Hz, it provides deeper filtering not only of the fundamental harmonic (31.5 Hz) but also effectively suppresses the high-frequency "noise" (63 Hz and above), which is partially transmitted by the stiffer models A and B.

Influence of Perforation on Dynamic Characteristics
The analysis showed that introducing perforation into the body of the vibration isolator is an effective tool for controlling stiffness without changing the overall dimensions of the isolator. A comparative analysis of the three configurations under a static load F_{stat} = 2000 kN revealed the following patterns:

1. Stiffness Reduction: The transition from the isolator without holes (Type A) to the perforated structure with five holes (Type C) led to an increase in static settlement from 10.2 mm to 22.1 mm. This indicates a reduction in the vertical static stiffness of the system by more than a factor of two.
2. The natural frequency of the loaded vibration isolator system shifted from 9.50 Hz (Type A) to 8.06 Hz (Type C). The reduction of 1.44 Hz is significant, as it allows for increased detuning from the dominant excitation frequencies.

Effectiveness of Vibration Protection in the Frequency Spectrum Excited by Subway Trains
Analysis of the transmission ratio (TR) for the main excitation frequency of 31.5 Hz (peak of the vibration spectral density) demonstrated the high efficiency of the proposed solution:

$$TR \sim \left|\frac{1}{1-\eta^2}\right|, \text{где } \eta = \frac{f_{ext}}{f_n} \quad (25)$$

For all isolator types, the condition for post-resonance operation is met:

$$\eta = f_{ext}/f_n \quad (26)$$

The frequency ratio is η ≈ 3.3 for the solid block and increases to η ≈ 3.9 for the perforated one (Type C). The calculated transmission ratio for Type C was TR ≈ 0.07, corresponding to a vibration level reduction of 23 dB. This surpasses the performance of the solid vibration isolator (TR ≈ 0.10, 20 dB) and confirms the feasibility of using perforation [21].

Nonlinear Effects
Accounting for geometric nonlinearity and material hyperelasticity allowed for the identification of the rubber "stiffening" effect under large deformations. Ignoring this effect would lead to an incorrect assessment of vibration isolation efficiency and errors in predicting resonant frequencies.

6. CONCLUSIONS

This work presents a nonlinear dynamic simulation of a rubber-metal vibration isolator subjected to a static load from a building and dynamic excitation caused by vibrations from a shallow underground railway. The main conclusions of the study are as follows:

1. The introduction of a system of five vertical holes (1 central + 4 peripheral) allows for a reduction in the natural frequency of the vibration isolator to 8.06 Hz. This ensures reliable protection against the critical frequency range (31.5 Hz – 63 Hz).
2. The developed configuration provides a transmission ratio of TR ≈ 0.07 at the dominant frequency. In the frequency range of 31.5–63 Hz, characteristic of vibrations from shallow subway systems, a reduction in vibration levels by more than a factor of 10 is achieved for a building located near a shallow underground railway.
3. It is demonstrated that the application of simplified linear models is inadmissible when using rubber-metal vibration isolators. The use of the Mooney-Rivlin model and the consideration of large displacements revealed a significant difference between the actual dynamic stiffness and linear extrapolation, confirming the necessity of employing the developed algorithm (Newmark method + Newton-Raphson iterations).

The contribution of this study in practice lies in substantiating the choice of the vibration isolator configuration (Type C), which provides an optimal balance between load-bearing capacity (up to 2000 kN) and the required effective compliance for suppressing low-frequency vibrations generated by trains in shallow subway systems.

7. ACKNOWLEDGEMENT

The work was funded by the Ministry of Science and Higher Education of the Russian Federation, project No. FSWG-2023-0004.

REFERENCES

1. **M. Kaliske, H. Rothert** (1997) Formulation and implementation of three-dimensional viscoelasticity at small and finite strains. Computational Mechanics 19 228-239. https://doi.org/10.1007/s004660050171
2. **Hamid Reza Ghoreishy** (2012) Determination of the parameters of the Prony series in hyper-viscoelastic material models using the finite element method. Materials & Design Volume 35, 791-797. https://doi.org/10.1016/j.matdes.2011.05.057
3. **Li Z., Lou J** (2011) Simulation on Performance of Rubber Isolator Based on ANSYS. 2nd International Conference on Mechanic Automation and Control Engineering, MACE 2011 - Proceedings. DOI:10.1109/MACE.2011.5987260
4. **A.J.M. Ferreira, J.M.A.C. Sá, A.T. Marques** (2003) Nonlinear Finite Element Analysis of Rubber Composite Shells ISSN 0556-171X. Проблемы прочности, № 3, УДК 539.4. DOI: 10.1023/A:1024656604257
5. **Mondrus V.L., Sizov D.K., Kvasnikov T.M.** (2023) Raschet rezinometallicheskih vibroizolyatorov s otverstiyami v sisteme vibrozashchity zdanij s pomoshch'yu programmnogo kompleksa, realizuyushchego metod konechnyh elementov [Finite Element Modelling of Rubber-Metal Vibration Isolators with Holes for the Vibration Protection System of Buildings]// ZHelezobetonnye konstrukcii. [Reinforced concrete structures]4(4):43-51. (In Russian) https://doi.org/10.22227/2949-1622.2023.4.43-51
6. **H. Sugihardjo, Y. Lesmana** (2018) FE Model of Low Grade Rubber for Modeling Housing's Low-Cost Rubber Base Isolators. Civil Engineering Journal. 4. 24. https://doi.org/10.28991/cej-030966
7. **Nidhal Jridi, M. Arfaoui** (2018) The capability of three separable finite-strain viscoelastic models to predict response of a filled

rubber material. Mechanics & Industry, Volume 19, Number 5. https://doi.org/10.1051/meca/2018014
8. **Wang, Rui & Li, Shiqi & Song, Shaoyun**. (2007). A Viscohyperelastic Constitutive Model for Rubber Used in Vibration Isolation. Noise & Vibration Worldwide. 38. 12-19. DOI 10.1260/095745607783360262.
9. **Hedayati Dezfuli, Farshad & Alam, M. Shahria.** (2012). Material Modeling of High Damping Rubber in Finite Element Method. Proceedings, Annual Conference - Canadian Society for Civil Engineering. 3.
10. **Tapia Romero, Manuel Alejandro & Gomez, Mariamne & Lugo, Luis**. (2020). Prony series calculation for viscoelastic behavior modeling of structural adhesives from DMA data. Ingeniería Investigación y Tecnología. 21. 1-10. DOI 10.22201/fi.25940732e.2020.21n2.014.
11. **Wu, Yifeng & Wang, Hao & Li, Aiqun.** (2016). Parameter Identification Methods for Hyperelastic and Hyper-Viscoelastic Models. Applied Sciences. 6. 386. DOI 10.3390/app6120386.
12. **Kartik Srinivas** (2020) Hyperelastic and Viscoelastic Characterization of Polymers and Rubber Materials Advanced Scientific and Engineering Services (AdvanSES)
13. **Lee, W.-S & Youn, Sung-Kie.** (2004). Topology optimization of rubber isolators considering static and dynamic behaviours. Structural and Multidisciplinary Optimization. 27. 284-294. DOI 10.1007/s00158-004-0376-1.
14. **Beijers, Clemens & de Boer, Andre.** (2003). Numerical modelling of rubber vibration isolators. Tenth International Congress on Sound and Vibration, Stockholm, Sweden
15. **Chip Fricke** (2013) Nonlinear Analysis Using Femap with NX Nastran. FEMAP SYMPOSIUM 2013 Mission Critical Design and Analysis
16. Rahnavard, Rohola & Craveiro, Hélder & Napolitano, Rebecca. (2020). Static and dynamic stability analysis of a steel-rubber isolator with rubber cores. Structures. 26. 441-455. DOI 10.1016/j.istruc.2020.04.048.
17. **Johnson & Chen** (2003) An Approximate Dissipation Function for Large Strain Rubber Thermo-Mechanical Analyses. NASA/TM-2003-212430
18. **Simo & Hughes** (1998) Computational Inelasticity. Springer-Verlag NewYork, In
19. **Bathe, K.J.** (1996). Finite Element Procedures. PRENTICE HALL, Upper Saddle River, New Jersey 07458
20. **Schaefer R.J**. (2001) Chapter 33 Mechanical Properties of Rubber
21. **Dashevskij M.A., Mondrus V.L., Motorin V.V.** (2017) Effektivnaya vibrozashchita verhnego stroeniya puti metropolitena [Effective vibration protection of the superstructure of the subway track]/ / Academia. Arhitektura i stroitel'stvo. [Academia. Architecture and construction.]. №4.

СПИСОК ЛИТЕРАТУРЫ

1. **Kaliske M., Rothert H.** Formulation and implementation of three-dimensional viscoelasticity at small and finite strains // 1997. Computational Mechanics. 19. P. 228–239. DOI: 10.1007/s004660050171.
2. **Ghoreishy H.R.** Determination of the parameters of the Prony series in hyper-viscoelastic material models using the finite element method // 2012. Materials & Design. 35. P. 791–797. DOI: 10.1016/j.matdes.2011.05.057.
3. **Li Z., Lou J.** Simulation on performance of rubber isolator based on ANSYS // 2011. 2nd International Conference on Mechanic Automation and Control Engineering (MACE 2011): Proceedings. DOI: 10.1109/MACE.2011.5987260.
4. **Ferreira A.J.M., Sá J.M.A.C., Marques A.T.** Nonlinear finite element analysis of rubber composite shells // 2003. Проблемы прочности. № 3. УДК 539.4. DOI: 10.1023/A:1024656604257.

5. **Мондрус В.Л., Сизов Д.К., Квасников Т.М.** Расчет резинометаллических виброизоляторов с отверстиями в системе виброзащиты зданий с помощью программного комплекса, реализующего метод конечных элементов // Железобетонные конструкции. 2023,4(4):43-51 https://doi.org/10.22227/2949-1622.2023.4.43-51
6. **Sugihardjo H., Lesmana Y.** FE model of low grade rubber for modeling housing's low-cost rubber base isolators // 2018. Civil Engineering Journal. 4. P. 24. DOI: 10.28991/cej-030966.
7. **Jridi N., Arfaoui M**. The capability of three separable finite-strain viscoelastic models to predict response of a filled rubber material // 2018. Mechanics & Industry. 19. № 5. DOI: 10.1051/meca/2018014.
8. **Wang R., Li S., Song S**. A viscohyperelastic constitutive model for rubber used in vibration isolation // 2007. Noise & Vibration Worldwide. 38. P. 12–19. DOI: 10.1260/095745607783360262.
9. **Hedayati Dezfuli F., Alam M.S.** Material modeling of high damping rubber in finite element method // 2012. Proceedings, Annual Conference - Canadian Society for Civil Engineering. 3.
10. **Tapia Romero M.A., Gomez M., Lugo L.** Prony series calculation for viscoelastic behavior modeling of structural adhesives from DMA data // 2020. Ingeniería Investigación y Tecnología. 21. P. 1–10. DOI: 10.22201/fi.25940732e.2020.21n2.014.
11. **Wu Y., Wang H., Li A**. Parameter identification methods for hyperelastic and hyper-viscoelastic models // 2016. Applied Sciences. 6. P. 386. DOI: 10.3390/app6120386.
12. **Srinivas K.** Hyperelastic and viscoelastic characterization of polymers and rubber materials // 2020. Advanced Scientific and Engineering Services (AdvanSES).
13. **Lee W.-S., Youn S.-K.** Topology optimization of rubber isolators considering static and dynamic behaviours // 2004. Structural and Multidisciplinary Optimization. 27. P. 284–294. DOI: 10.1007/s00158-004-0376-1.
14. **Beijers C., de Boer A.** Numerical modelling of rubber vibration isolators // 2003. Tenth International Congress on Sound and Vibration, Stockholm, Sweden.
15. **Beijers C., de Boer A.** Numerical modelling of rubber vibration isolators // 2003. Tenth International Congress on Sound and Vibration, Stockholm, Sweden.
16. **Rahnavard R., Craveiro H., Napolitano R.** Static and dynamic stability analysis of a steel-rubber isolator with rubber cores // 2020. Structures. 26. P. 441–455. DOI: 10.1016/j.istruc.2020.04.048.
17. **Johnson, Chen.** An approximate dissipation function for large strain rubber thermo-mechanical analyses // 2003. NASA/TM-2003-212430.
18. **Simo, Hughes**. Computational inelasticity // 1998. Springer-Verlag, New York.
19. **Bathe K.J.** Finite element procedures // 1996. Prentice Hall, Upper Saddle River, New Jersey 07458.
20. **Schaefer R.J.** Chapter 33 mechanical properties of rubber // 2001.
21. **Дашевский М.А., Мондрус В.Л., Моторин В.В.** Эффективная виброзащита верхнего строения пути метрополитена // Academia. Архитектура и строительство. 2017. №4.

Mondrus Vladimir Lvovich – Doctor of Technical Sciences, Professor, Corresponding Member. RAASN, Professor of the Department of Structural and Theoretical Mechanics, Institute of Industrial and Civil Engineering, National Research Moscow State University of Civil Engineering (NRU MGSU). 405, 26 Yaroslavskoe highway, Moscow, 129337, Russia. E-mail: mondrusvl@mgsu.ru

Мондрус Владимир Львович – д.т.н., профессор, член корр. РААСН, профессор кафедры строительной и теоретической механики, институт Промышленного и гражданского строительства, Национальный Исследовательский Московский Государственный Строительный Университет (НИУ МГСУ). 405, 26 Ярославское шоссе, Москва, 129337, Россия. E-mail:mondrusvl@mgsu.ru

Sizov Dmitry Konstantinovich – Ph.D., Vibroseysmozashchita LLC,6 st. Bratislavskaya, Moscow, 109341, Russia. E-mail: newfff@mail.ru

Kvasnikov Timofei Mikhailovich - 4rd year graduate student of the Department of Structural and Theoretical Mechanics, Institute of Industrial and Civil Engineering, National Research Moscow State University of Civil Engineering (NRU MGSU). 405, 26 Yaroslavskoe shosse, Moscow, 129337, Russia. E-mail: tima.kvasnikov@gmail.com, https://orcid.org/0000-0002-7836-4918

Сизов Дмитрий Константинович – к.т.н., ООО «Вибросейсмозащита»,ул. Братиславская, 6, Москва, 109341,Россия. E-mail: newfff@mail.ru

Квасников Тимофей Михайлович -аспирант 4 курса кафедры строительной и теоретической механики, институт Промышленного и гражданского строительства, Национальный Исследовательский Московский Государственный Стро-ительный Университет (НИУ МГСУ). 405, 26 Ярославское шоссе, Москва, 129337, Россия. E-mail: tima.kvasnikov@gmail.com, https://orcid.org/0000-0002-7836-4918